



HAL
open science

Quasi-Global Maps of Daily Aerosol Optical Depth From a Ring of Five Geostationary Meteorological Satellites Using AERUS-GEO

Xavier Ceamanos, Bruno Six, J. Riedi

► **To cite this version:**

Xavier Ceamanos, Bruno Six, J. Riedi. Quasi-Global Maps of Daily Aerosol Optical Depth From a Ring of Five Geostationary Meteorological Satellites Using AERUS-GEO. *Journal of Geophysical Research: Atmospheres*, 2021, 126 (20), pp.e2021JD034906. 10.1029/2021jd034906 . hal-03403043

HAL Id: hal-03403043

<https://hal.univ-lille.fr/hal-03403043v1>

Submitted on 26 Oct 2021

HAL is a multi-disciplinary open access archive for the deposit and dissemination of scientific research documents, whether they are published or not. The documents may come from teaching and research institutions in France or abroad, or from public or private research centers.

L'archive ouverte pluridisciplinaire **HAL**, est destinée au dépôt et à la diffusion de documents scientifiques de niveau recherche, publiés ou non, émanant des établissements d'enseignement et de recherche français ou étrangers, des laboratoires publics ou privés.



Distributed under a Creative Commons Attribution 4.0 International License



RESEARCH ARTICLE

10.1029/2021JD034906

Key Points:

- Quasi-global maps of aerosol properties are retrieved from a combination of five geostationary meteorological satellites
- The algorithm AERUS-GEO is used to retrieve daily-averaged aerosol optical depth from the satellite observations
- The retrieved aerosol data have strong potential to improve global aerosol forecasting and to monitor long-range-transported aerosols

Correspondence to:

X. Ceamanos,
xavier.ceamanos@meteo.fr

Citation:



Ceamanos, X., Six, B., & Riedi, J. (2021). Quasi-global maps of daily aerosol optical depth from a ring of five geostationary meteorological satellites using AERUS-GEO. *Journal of Geophysical Research: Atmospheres*, 126, e2021JD034906. <https://doi.org/10.1029/2021JD034906>

Received 23 MAR 2021
Accepted 28 SEP 2021

© 2021. The Authors.

This is an open access article under the terms of the [Creative Commons Attribution-NonCommercial-NoDerivs License](https://creativecommons.org/licenses/by/4.0/), which permits use and distribution in any medium, provided the original work is properly cited, the use is non-commercial and no modifications or adaptations are made.

Quasi-Global Maps of Daily Aerosol Optical Depth From a Ring of Five Geostationary Meteorological Satellites Using AERUS-GEO

Xavier Ceamanos¹ , Bruno Six², and Jérôme Riedi^{2,3} 

¹CNRM, Météo-France, CNRS, Université de Toulouse, Toulouse, France, ²University of Lille, CNRS, CNES, UMS 2877 – ICARE Data and Services Center, F-59000 Lille, France, ³University of Lille, CNRS, UMR 8518 – LOA – Laboratoire d'Optique Atmosphérique, F-59000 Lille, France

Abstract Geostationary meteorological satellites are recently receiving a great deal of attention from the aerosol remote sensing community due to their increasingly advanced performances including their ability to acquire multiple views of the Earth per day. However, this type of observing systems are limited by their partial coverage of the globe, which makes them inappropriate for monitoring long-range-transported particles or assimilating the derived aerosol products into global atmospheric models. This shortcoming is overcome in this pioneering investigation thanks to the simultaneous use of the geostationary satellites GOES-17, GOES-16, Meteosat-11, Meteosat-8, and Himawari-8. The combination of these five spacecrafts (herein referred to as GEO-ring) covers the full globe except for polar regions, which are not seen from geostationary orbit. Data acquired by the GEO-ring in 2020 are processed by the algorithm AERUS-GEO to provide quasi-global maps of daily aerosol optical depth (AOD). These data are proved to be accurate with respect to AERONET ground measurements. The potential of the GEO-ring for aerosol science is then demonstrated. First, retrieved AOD maps are proved to be potentially useful for global aerosol forecasting due to the improved Earth coverage of the GEO-ring with respect to the polar orbiting satellites Terra/Aqua (51.4% vs. 26.6%). Second, retrieved aerosol data are used to track long-range-transported aerosols emitted during the 2020 Western US wildfires. This article is a prelude to the aerosol remote sensing that will be possible when a GEO-ring exclusively consisting of next generation imagers will be available with the launch of Meteosat Third Generation-Imager.

1. Introduction

Aerosols consist of fine particles suspended in the atmosphere that are emitted by natural sources as well as human activities. Aerosols are of great importance in topics related to climate, weather forecasting, defense, air quality, photovoltaic energy, and air transport. Among their many impacts, it is well known that aerosols play a role in the Earth's radiation budget through their extinction of incident solar radiation (Ceamanos et al., 2014) and their complex interactions with clouds (Stevens & Feingold, 2009). The magnitude of aerosol effects depends on the concentration of particles and their chemical composition (i.e., the aerosol type), which can range from sulfate particles coming from volcanic eruptions to particulate air pollutants emitted from anthropogenic sources. Nowadays, there exist significant uncertainties on the spatial distribution and the temporal evolution of aerosols, which make it difficult to study their impacts at the regional and global scale (Boucher et al., 2013). Uncertainties may become particularly notable when aerosol particles are transported over long distances such as mineral dust blown out from the Sahara Desert reaching South America (Yu et al., 2015) or smoke emanated from Canadian wildfires traveling to northern France (Hu et al., 2019).

Spaceborne remote sensing is a unique tool for detecting, characterizing, and mapping aerosols, with optical imagers operating in the visible and near infrared (VNIR) spectral range being predominantly used for this purpose. Satellite observations are processed by retrieval algorithms that generally provide an estimate of the aerosol optical depth (AOD), which is linked to the particle content in the atmosphere (Wei et al., 2020). Spaceborne remote sensing of AOD is made possible through two types of platforms: polar orbiting satellites and geostationary satellites.

The former spacecrafts have been extensively used for aerosol remote sensing thanks to their moderate to high spatial resolution and their global coverage. The most popular instrument in AOD studies for the past years has been the MODerate resolution Imaging Spectroradiometer (MODIS) aboard the Terra and Aqua satellites thanks to the reliability of the derived aerosol products (Hsu et al., 2013; Levy et al., 2013; Lyapustin et al., 2018). The main shortcoming of polar orbiting spacecrafts such as Terra and Aqua is the low frequency of aerosol observations due to their one or two overpasses per day only.

Geostationary weather satellites are capable of overcoming this limitation thanks to their high temporal resolution (between four and six full-disk scans per hour), which makes them valuable for continuous monitoring of aerosols. The availability of multiple Earth views per day has two main advantages. First, it allows for an improved estimation of the surface bidirectional reflectance distribution function (BRDF), which is key in disentangling the aerosol signal from the satellite observations. Second, it provides a diversity of angular measurements that increases the chances of detecting and characterizing the aerosols at some moment of the day (Ceamanos, Moparthy, Carrer, & Seidel, 2019). The advantages of geostationary satellites for aerosol remote sensing were demonstrated by Xu et al. (2014) who found a higher number of satisfactory AOD estimates with respect to MODIS aerosol products for the AERUS-GEO (Aerosol and surface albedo Retrieval Using a directional Splitting method-application to GEOstationary data) aerosol product. AERUS-GEO provides daily-averaged AOD and surface albedo from the Spinning Enhanced Visible Infra-Red Imager (SEVIRI) aboard the geostationary satellite Meteosat Second Generation (MSG; Carrer et al., 2010, 2014). Many other aerosol products exist for geostationary satellites around the globe such as MSG (Govaerts et al., 2010; Thieuleux et al., 2005), the series of Geostationary Operational Environmental Satellites (GOES; Knapp, 2002; Kondragunta et al., 2020), Himawari (Gupta et al., 2019; Lim et al., 2018; Yoshida et al., 2018), and the Geostationary Ocean Color Imager (GOCI; Choi et al., 2016). The main weakness of this type of spacecrafts is that their coverage is limited to the Earth's disk that is seen from the geostationary orbit. This limitation makes the use of a single geostationary satellite ineffective for some applications such as the monitoring of long-range-transported aerosols or the assimilation of the resulting AOD products into global atmospheric models.

This article discusses and demonstrates the potential of simultaneously exploiting an ensemble of geostationary meteorological satellites to obtain a single aerosol observation covering the majority of the Earth (polar regions not being seen from the geostationary orbit). This is possible thanks to the so-called geostationary ring (referred to as GEO-ring hereafter), which is a constellation of several geostationary satellites evenly located around the planet. Today, a meteorological GEO-ring is possible thanks to the simultaneous use of the Advanced Baseline Imager (ABI) on GOES-16 and GOES-17 from the National Oceanic and Atmospheric Administration (NOAA; Schmit et al., 2017), the Advanced Himawari Imager (AHI) on the Himawari-8 spacecraft from the Japan Meteorological Agency (JMA; Bessho et al., 2016), and the SEVIRI instrument aboard the MSG spacecrafts from the European Organization for the Exploitation of Meteorological Satellites (EUMETSAT; Schmetz et al., 2002). Despite the proven capabilities of each individual satellite to monitor aerosols, the potential of the GEO-ring to provide a quasi-global coverage of the Earth has been rarely investigated to our knowledge. We can cite the work of Xie et al. (2020), who processed data acquired from four geostationary satellites with different retrieval algorithms to estimate AOD over land only, and the work of Remer et al. (2020), who briefly illustrated the combination of AOD maps retrieved by the Dark Target (DT) algorithm from geostationary and polar orbiting satellites. Other works have addressed the fusion of geostationary aerosol products over specific regions such as Lim et al. (2021), who integrated GOCI and AHI data to estimate AOD over East Asia based on a data fusion approach.

The objective of this article is to assess the potential for aerosol studies of a GEO-ring made of five weather geostationary missions evenly located around the Earth: GOES-West at 137.2°W (with GOES-17 satellite) over the Eastern Pacific Ocean, GOES-East at 75.2°W (with GOES-16 satellite) over America, the operational MSG at 0° (with Meteosat-11 satellite) over Europe and Africa, the former MSG at 41.5°E known today as Indian Ocean Data Coverage (IODC; with Meteosat-8 satellite) over the Indian Ocean, and Himawari at 140.7°E (with Himawari-8 satellite) over East Asia and Oceania. The location and coverage of each satellite is given in Figure 1. In order to meet this objective, the retrieval algorithm AERUS-GEO was adapted to process each geostationary satellite forming the considered GEO-ring. The choice of this algorithm is justified based on the reliability of daily AOD values retrieved by AERUS-GEO with respect to Aerosol Robotic

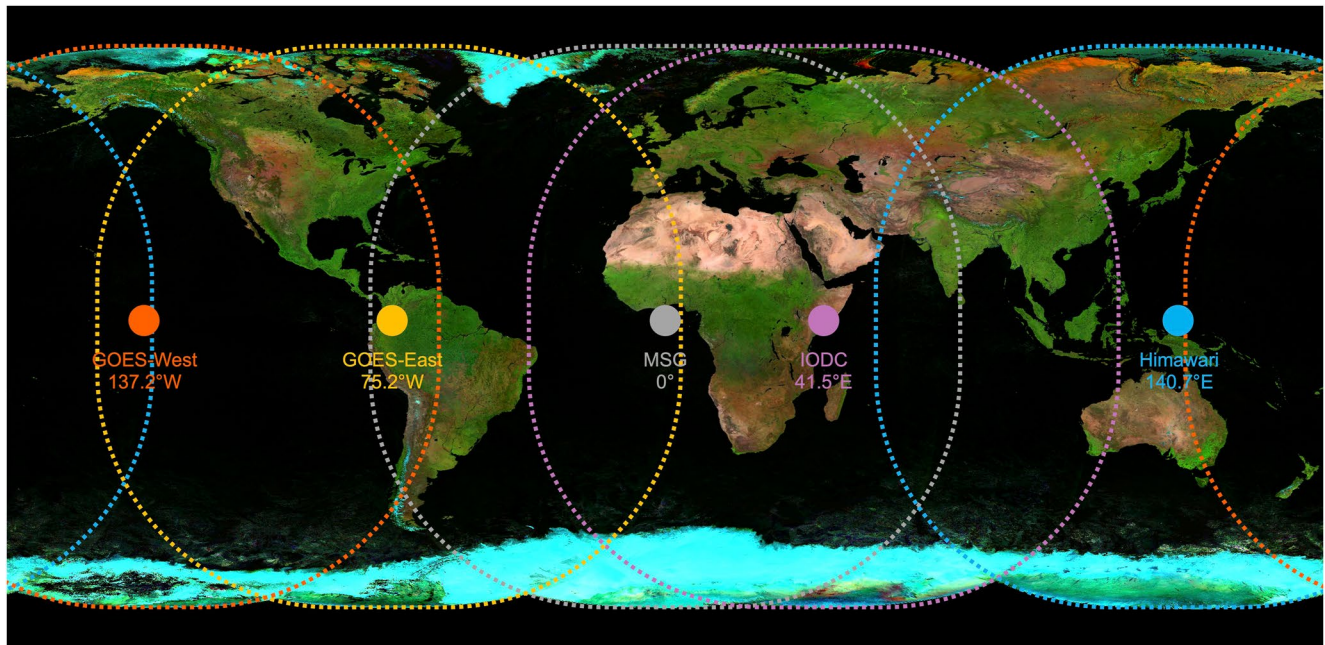


Figure 1. Subsatellite point and coverage of the five geostationary weather satellites forming the GEO-ring considered in this study. The background image corresponds to the spectral surface albedo obtained by AERUS-GEO from the GEO-ring on September 18, 2020. The color composite is obtained by combining the albedo estimated for spectral channels VIS06 (in blue), VIS08 (in green), and IR016 (in red).

Network (AERONET) ground measurements and other satellite products, as it was shown in several studies (Escribano et al., 2017; Nabat et al., 2015; Xu et al., 2014). The quality of the estimates of daily-averaged AOD retrieved in this work from the GEO-ring was also assessed against collocated aerosol properties obtained from AERONET stations. Quasi-global maps of daily AOD were then derived by combining the individual satellite retrievals. The potential of the resulting data, and thus of a GEO-ring of meteorological satellites, for aerosol studies is illustrated in this work by focusing on the intercontinental transport of smoke particles emitted by the extensive wildfires that occurred in Western United States (US) in late summer 2020. Furthermore, the value of the GEO-ring aerosol products for aerosol forecasting using global atmospheric models is illustrated with respect to the generally assimilated aerosol products based on polar orbiting imagers.

This article is organized as follows. Section 2 summarizes the theoretical basis and implementation of the AERUS-GEO retrieval algorithm, the required inputs, and the latest improvements. Section 3 details the data that were used in this work, the adaptation of AERUS-GEO to the different geostationary satellites, and the fusion of the retrieved maps of daily AOD into a global data set. Section 4 details the evaluation of the GEO-ring AOD retrievals against other aerosol data (*in situ*, model-based, and satellite-derived), as well as their use for tracking long-range-transported particles. The potential of the GEO-ring for the study of aerosols is discussed in Section 5 and conclusions are drawn in Section 6.

2. Methods

2.1. Summary of AERUS-GEO Algorithm

AERUS-GEO is a retrieval algorithm that provides estimates of daily-averaged total AOD and surface albedo from VNIR geostationary observations (Carrer et al., 2010, 2014). It uses as input data:

1. Full-disk images of top-of-atmosphere radiances measured during the day for spectral channels centered on 0.6, 0.8, and 1.6 μm (hereafter referred to as VIS06, VIS08, and IR016).
2. Solar and view angles including solar zenith angle (θ_s), view zenith angle (θ_v), and relative azimuth angle (φ_r).
3. Binary cloud mask to limit the processing to cloud-free pixels only.

4. Fields of surface pressure, total column water vapor, and total column ozone.
5. Static files including latitude, longitude, land–water mask, and a digital elevation model.

The retrieval scheme of AERUS-GEO is composed of two main steps:

1. Cloud-free radiance observations are first corrected for molecular effects (i.e., gas absorption and Rayleigh scattering) using the Simplified Model for Atmospheric Correction (SMAC; Rahman & Dedieu, 1994). SMAC performs an efficient correction for O₂, CO₂, N₂O, CH₄, H₂O, and O₃ based on parametric equations that are fitted using accurate radiative transfer simulations. Atmospheric gases are set to the standard concentration values defined in the US Standard 62 model. However, forecasts or analyses of total column water vapor and total column ozone are used by SMAC to refine the characterization of the state of the atmosphere, as these species show a strong absorption in the VNIR range. Surface pressure is also required by SMAC as input to take into account the variation of surface height. The accuracy of SMAC is within 2% and 3%, if slope effects are mild and large viewing and solar angles are avoided.
2. Corrected reflectances are then aggregated at the end of the day for every pixel of the satellite images to perform simultaneous retrieval of daily-averaged AOD and surface BRDF. This is achieved by the mathematical inversion of an analytical radiative transfer model (RTM) that is fitted with the available satellite observations. The RTM uses four kernels to represent the dependence on solar and viewing geometry of the reflectance of surfaces and aerosols. The dependence of the former signal is taken into account through the surface BRDF, which is represented using the three kernels of the Ross-Thick Li-Sparse (RTLS) model (Lucht et al., 2000). The angular dependence of aerosol reflectance—the fourth kernel—is taken into account through a Henyey–Greenstein scattering phase function. The unknown variables of the RTM are the multiplying factors of the four kernels, with AOD being the unknown variable for the aerosol kernel. The usually distinct angular properties between surfaces and aerosols are used to disentangle the two signals based on a full day of observations, which span a broad range of SZA values thanks to the geostationary orbit. This results in the estimation of the surface BRDF (i.e., the multiplying factors of the three RTLS kernels) and the AOD, which is supposed to be invariant during the day to reduce the number of unknown variables. Each daily retrieval is constrained using a Kalman filter (KF) that allows the consideration of the lastly available estimate of surface BRDF as a priori information. The KF is used to impose the usually slow variation of surface BRDF with time, while the AOD is allowed to change from day to day. Surface albedo is obtained from the angular integration of the retrieved surface BRDF.

More details on the retrieval method can be found in Carrer et al. (2010, 2014).

2.2. Recent Improvements

The algorithm AERUS-GEO was improved in the framework of the present investigation as follows:

1. SEVIRI radiances from Meteosat-11 and Meteosat-8 were recalibrated to take into account the systematic biases found by Meirink et al. (2013). In that work, an average bias of –8% was found for the SEVIRI channel VIS06 with respect to MODIS based on regressions of collocated near-nadir reflectance measurements. Recalibration coefficients take into account the different spectral response between MODIS and SEVIRI as they were calculated after converting the reflectances of the latter imager to the spectral response of MODIS.
2. Molecular correction was improved by updating the fitting coefficients used in SMAC. Coefficients were recalculated for each geostationary imager using radiative transfer simulations obtained with the code 6SV1 (Kotchenova et al., 2006), which includes many improvements with respect to the previously used code (i.e., 6S).
3. Satellite observations highly affected by sun glint were filtered out to avoid AOD overestimation. This was achieved by not processing water pixels with a glint angle α lower than 35° with α defined as

$$\cos \alpha = \cos \theta_s \cos \theta_v - \sin \theta_s \sin \theta_v \cos \varphi_r. \quad (1)$$

This filtering significantly improved the obtained maps of daily AOD and although it removes a large circular area from each full-disk scan (as it was noticed by Gupta et al. [2019]), the daily-averaged AOD maps do not exhibit specific regions of missing values as the glint affected area moves during the day.

Table 1
Characteristics of the Geostationary Meteorological Missions Forming the GEO-Ring Considered in This Study

Mission	Satellite (in 2020)	Position	Imager	Central wavelength (μm)	Bandwidth (FWHM ^a ; nm)	SNR ^a	Spatial resolution at s.s.p. ^a (km)	Scanning frequency (min)
GOES-West	GOES-17	137.2°W	ABI	0.640	64	>300	0.5–2.0	10
GOES-East	GOES-16	75.2°W	ABI	0.640	64	>300	0.5–2.0	10
MSG	Meteosat-11	0°	SEVIRI	0.635	71	>30	3.0	15
IODC	Meteosat-8	41.5°E	SEVIRI	0.635	71	>30	3.0	15
Himawari	Himawari-8	140.7°E	AHI	0.645	82	>300	0.5–2.0	10

Note. Central wavelength, bandwidth, SNR, and spatial resolution are given for channels VIS06. Data from Schmetz et al. (2002), Bessho et al. (2016), and Schmit et al. (2017).

^as.s.p. stands for subsatellite point, FWHM stands for full width at half maximum, and SNR stands for signal-to-noise ratio.

- The surface BRDF for each pixel is updated and propagated in time only when 3 hr of valid satellite observations are available for a given date. This improvement helped to obtain a more robust BRDF in time than with the previous version of the AERUS-GEO algorithm, which updated the BRDF solution anytime a single observation was available.
- Daily AOD maps were improved by spatial smoothing similarly to what is done in the Multi-Angle Implementation of Atmospheric Correction algorithm (Lyapustin et al., 2018). First, AOD maps were filtered using a running window that finds excessively high AOD values with respect to neighboring retrievals. Second, a running averaging window was applied to the resulting daily AOD maps. The window size was set to 10×10 km at the subsatellite point while it was allowed to increase for higher latitudes to take into account the variable spatial resolution of the geostationary projection grid. This resulted in smoothing windows of 15×15 km over Europe and North America. This step improved residual errors that are local and spatially coherent based on the assumption that aerosols are spatially homogeneous.
- Some minor bugs were fixed including the correction of a spatial artifact in the Southern Hemisphere coming from a wrong processing of azimuth viewing angles.

All algorithm refinements described above were proven to contribute to the improvement of the daily AOD retrievals in terms of accuracy, smoothness, and completeness.

3. Experimental Setup and Data

3.1. Application of AERUS-GEO to the GEO-Ring

In the past years, AERUS-GEO has been applied to observations of the SEVIRI instrument aboard the MSG geostationary mission at 0° to provide maps of daily AOD at 0.635 μm , which corresponds to the SEVIRI visible channel (VIS06). By daily AOD, we mean the AOD averaged over the clear-sky instants of a given date defined in Coordinated Universal Time (UTC). This definition handles the date line problem for Himawari-8 and GOES-West in the same way that is done for calculating daily averages of AOD from AERONET stations close to the international date line. The operational processing of SEVIRI data is performed by the Data and Services Center AERIS/ICARE since 2014 (Carrer et al., 2014; <https://www.icare.univ-lille.fr/projects/user-driven-projects/aerus-geo/>). The accuracy of the AERUS-GEO aerosol product was proved to be comparable to other satellite-derived AOD products by Xu et al. (2014). In that study, AERUS-GEO showed a similar precision with respect to aerosol retrievals from MODIS and the Multi-Angle Imaging Spectroradiometer over 24 AERONET stations. Since its release in 2014, AERUS-GEO has been used by the scientific community working on the study of aerosols in Europe (e.g., Gomez-Amo et al., 2017) and Africa (e.g., Roberts et al., 2018).

Recently, the AERUS-GEO algorithm was adapted to process VNIR observations from all the imagers forming the GEO-ring considered in this article. The relevant characteristics of each geostationary mission and imager such as spatial resolution and signal-to-noise ratio (SNR) are given in Table 1. AERUS-GEO was

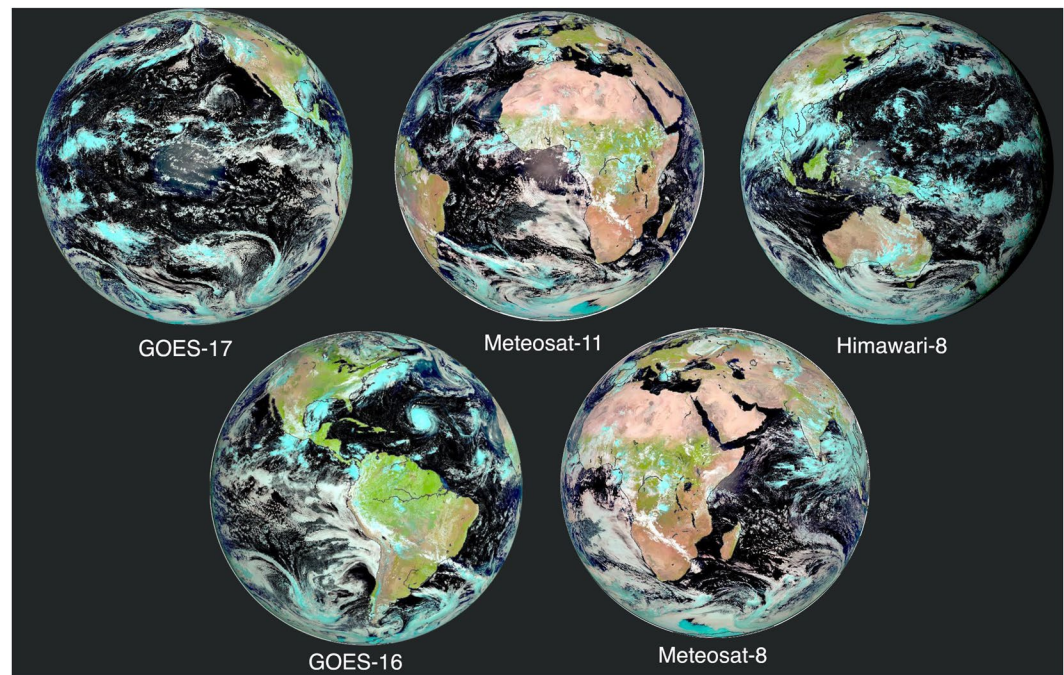


Figure 2. Color composites of spectral radiance on September 18, 2020, at noon for each of the five geostationary satellites. Blue, green, and red colors are assigned to channels VIS06, VIS08, and IR016, respectively.

set up to retrieve the daily-averaged AOD from each VIS06-equivalent channel. The choice of 640 nm for AOD retrievals is justified by the fact that VIS06 is the channel with the shortest wavelength common to all imagers. Spectral extrapolation of AOD to the usual 550 nm wavelength was not done due to its complexity, as it is corroborated by other studies retrieving AOD from SEVIRI at 635 nm only (e.g., Bernard et al., 2011; Thieuleux et al., 2005; Zawadzka-Manko et al., 2020). Spectral channels centered at 0.8 and 1.6 μm (VIS08 and IR016) were also processed by AERUS-GEO to calculate surface albedo (not evaluated in this article). It is important to note that VIS06, VIS08, and IR016 are the only channels in the VNIR range that are common to all imagers. Albeit other channels from ABI and AHI would obviously help improving aerosol retrievals, we made the decision to use an algorithm that is appropriate for all imagers. The choice of a single aerosol algorithm was made to obtain equivalent—and thus more easily mergeable—AOD maps, thus avoiding potential discontinuities among satellites in the quasi-global product. Figure 2 shows color composites created from the radiances of the three common channels for the five geostationary platforms on September 18, 2020, at noon. The spatial resolution of the new generation of imagers ABI and AHI ranges between 0.5 and 2 km for the VNIR channels. In this study, the data of these two imagers were set to a resolution of 2 km to reduce the processing time. This value was considered to be sufficient in regards of the SEVIRI nominal resolution of 3 km. The maximum scanning frequency was considered for MSG, IODC, and GOES-East, with full-disk scans every 15, 15, and 10 min, respectively. By contrast, the data of GOES-West and Himawari used in this study were available at a reduced frequency, every 30 and 20 min, respectively. The different temporal and spatial resolutions of each geostationary mission were considered in the adaptation of the retrieval algorithm. Specific SMAC coefficients for each satellite—obtained by convolving 6SV1 simulations with the corresponding spectral response function—were used for molecular correction. Finally, satellite data corresponding to solar and viewing zenith angles higher than 85° were discarded to avoid high airmass values leading to the usually degraded accuracy of RTM for these geometries.

3.2. Data Fusion

Quasi-global maps of aerosol properties were constructed by combining the outputs of AERUS-GEO obtained from each geostationary satellite. An equirectangular plate carrée projection with a spatial resolution of 0.1° was chosen. The daily-averaged AOD values were assigned to this global projection using a nearest

neighbor technique. In particular, each cell of the equirectangular grid was initially filled with the nearest AOD value from each satellite falling into the $0.1^\circ \times 0.1^\circ$ area defined by the grid cell. By nearest we mean the AOD value corresponding to the closest coordinates with respect to the center of the grid cell. A weighted average was then used for grid cells with several AOD values coming from different satellites. Averaging weights were set to the value of $\cos \theta_v$, θ_v being the VZA corresponding to the AOD estimate from each satellite—in order to provide smooth spatial transitions between satellites and reduce the error of the resulting quasi-global AOD map. This fusion technique is equivalent to the approach adopted by Xie et al. (2020). In practice, the dependence of weights on $\cos \theta_v$ contributed to reducing the VZA cutoff, as AOD values retrieved under high zenith angles were rarely used to construct the quasi-global maps. This helped accounting for (a) the usually degraded accuracy of RTM for long atmospheric paths and due to the sphericity of the Earth, and (b) the coarser resolution of AOD retrievals along the outer edge of the geostationary grid. The adopted merging approach provided similar results with respect to other more sophisticated algorithms that were tested in this study such as the Maximum Likelihood Estimate approach (e.g., Lim et al., 2021).

3.3. Data Sets Used for This Study

The following ancillary data were used in this investigation for the processing of the five geostationary satellites:

1. Cloud masks were obtained using the software from the EUMETSAT Satellite Application Facility on Support to Nowcasting and Very Short Range Forecasting (NWC SAF) program (<http://www.nwcsaf.org/>). This software estimates several cloud properties from satellite radiance observations using the current version of the algorithm of Derrien and Le Gleau (2005).
2. Atmospheric meteorological state parameters were obtained from near-real-time forecasts of the European Centre for Medium-Range Weather Forecasts (ECMWF). The original 3-hourly fields from ECMWF were temporally interpolated to match the frequencies from the geostationary imagers.

The experiments in this study were conducted using satellite observations spanning from February to September 2020. The improved version of the AERUS-GEO algorithm was used to process the data corresponding to the five geostationary satellites for this period of time. The processing of the first four months (February–May) was used as spin up time to allow the KF-based recursive method to provide reliable estimates of surface BRDF globally (Carrer et al., 2018). The results analyzed in Section 4 were therefore based on the maps of daily AOD obtained from June to September. It is important to note that the daily update of surface BRDF continued throughout the validation period to retrieve the natural evolution of BRDF with time. All the ancillary and satellite data used in this study were made available from February to September 2020 through the AERIS/ICARE archive.

3.4. Data Sets Used for AOD Validation

3.4.1. AERONET

The satellite AOD retrievals provided by AERUS-GEO from the five geostationary satellites forming the GEO-ring were evaluated against aerosol inversions obtained from AERONET ground measurements. AERONET is a federated network of more than 600 autonomously operated Sun-sky photometers scattered around the world that are used to measure solar irradiance from which column-integrated aerosol properties are provided (Holben et al., 1998). The evaluation assessment was performed against all stations that were operational during the period from June to September 2020. AERONET data were processed by the latest Version 3 processing algorithm (Giles et al., 2019), which includes updated and improved cloud screening and quality control methods. The AERONET data used in this work corresponded to the quality Level 1.5, which includes automatic cloud-clearing but does not apply prefield or postfield calibration such as in Level 2.0. The reason for this choice was the scarcity of Level 2.0 data for most of stations for the period of study at the time of writing for this article. The original AOD daily averages at 675 nm from AERONET were converted to 640 nm using the Angstrom exponent calculated between 440 and 675 nm.

3.4.2. MODIS

The validity of the AERUS-GEO quasi-global aerosol outputs was also assessed using equivalent maps of total AOD provided by the MODIS imagers aboard the Terra and Aqua satellites. In particular, this investigation used the products MOD08_D3_v6.1 and MYD08_D3_v6.1, which is a Level 3 MODIS gridded atmosphere daily global joint product. We used the statistical data set (SDS) named *AOD_550_Dark_Target_Deep_Blue_Combined* interpolated at a resolution of 0.1° that is provided by the NASA Earth Observations (NEO; <https://neo.sci.gsfc.nasa.gov/>). This SDS results from the combination of the DT and Deep Blue (DB) algorithms (Hsu et al., 2013; Levy et al., 2013) and was chosen to maximize the AOD coverage. On the one hand, DT uses a set of ratios and relationships between the 0.47, 0.67, and $2.1\ \mu\text{m}$ channels to account for the surface signal. This method works best over dark vegetated targets and does not work over bright land surfaces. On the other hand, DB uses maps and libraries of surface reflectance in the blue channels to account for the surface signal as well as spectral reflectance ratios. This method works best over bright land surfaces but can also retrieve aerosols over most vegetated targets. The combined DT and DB products used in this work (hereafter referred to as DT-DB) provided total AOD at 550 nm from Terra (with an overpass time around 10:30 a.m.) and Aqua (with an overpass time around 1:30 p.m.).

3.4.3. Copernicus Atmosphere Monitoring Service

The satellite AOD maps derived from the GEO-ring were also compared to forecasts from the Copernicus Atmosphere Monitoring Service (CAMS; <https://atmosphere.copernicus.eu/>). ECMWF produces CAMS aerosol properties with a comprehensive Earth system model named Integrated Forecast System (IFS; <https://www.ecmwf.int/en/publications/ifs-documentation>). The aerosol module of IFS is a bulk-bin scheme simulating five types of aerosols with 12 prognostic tracers (Benedetti et al., 2009; Morcrette et al., 2009; Rémy et al., 2019). There are three size bins for sea salt ($0.03\text{--}0.5$, $0.5\text{--}0.9$, and $0.9\text{--}20\ \mu\text{m}$), similarly three bins for dust ($0.03\text{--}0.5$, $0.5\text{--}0.9$, and $0.9\text{--}20\ \mu\text{m}$), organic matter, and black carbon with the hydrophilic and hydrophobic component, sulfur dioxide, and sulfate aerosol. CAMS forecasts assimilate satellite AOD estimates of MODIS/Terra, MODIS/Aqua, as well as the Polar Multi-sensor Aerosol properties (PMAp) product derived from the EUMETSAT MetOp polar orbiting satellites (Popp et al., 2016). The CAMS variables used in this article consisted of forecasted total AOD at 670 nm at noon.

4. Results

4.1. Daily AOD Retrievals From Five Geostationary Satellites

The results obtained by AERUS-GEO from the five geostationary weather satellites forming the GEO-ring are illustrated in Figure 3. This figure shows the maps of daily-averaged AOD at 640 nm that were obtained for September 18, 2020. These data outputs show several massive aerosol plumes including desert dust blowing out from Northern Africa and smoke emitted by biomass burning in South America. Overall, the maps of daily AOD do not exhibit obvious spurious artifacts and are mostly complete, with gaps in regions that were cloudy during a significant fraction of the day on the selected date.

4.2. Evaluation Against AERONET Ground-Based Observations

Table 2 summarizes the results that were obtained in the assessment experiment by giving, for each satellite, the average correlation (r), the average mean bias error (MBE), and the average root mean squared error (RMSE) calculated from the coincident daily AOD estimates from AERUS-GEO and AERONET. All pairs of temporally collocated satellite and ground daily AOD values between June 1 and September 30 were considered. Average scores correspond to the mean over all pairs of AOD values. The regression line between the two data sets (y), the total number of values (N), the total number of stations (n), and the average daily AOD retrieved by AERONET ($\bar{r}_{AERONET}$) are also given. Finally, Table 2 provides the percentage of days with a successful AOD retrieval, which gives an indication of the temporal availability of the satellite product.

Table 2 shows a satisfactory agreement between AERUS-GEO and AERONET retrievals for all satellites, with a correlation between 0.69 and 0.80, an MBE between 0.01 and 0.02, and a RMSE between 0.10 and 0.16. The slope of the regression line varied between 0.69 and 0.96, which shows a slight underestimation for high aerosol concentrations. The scores obtained in this study are similar or slightly better than those

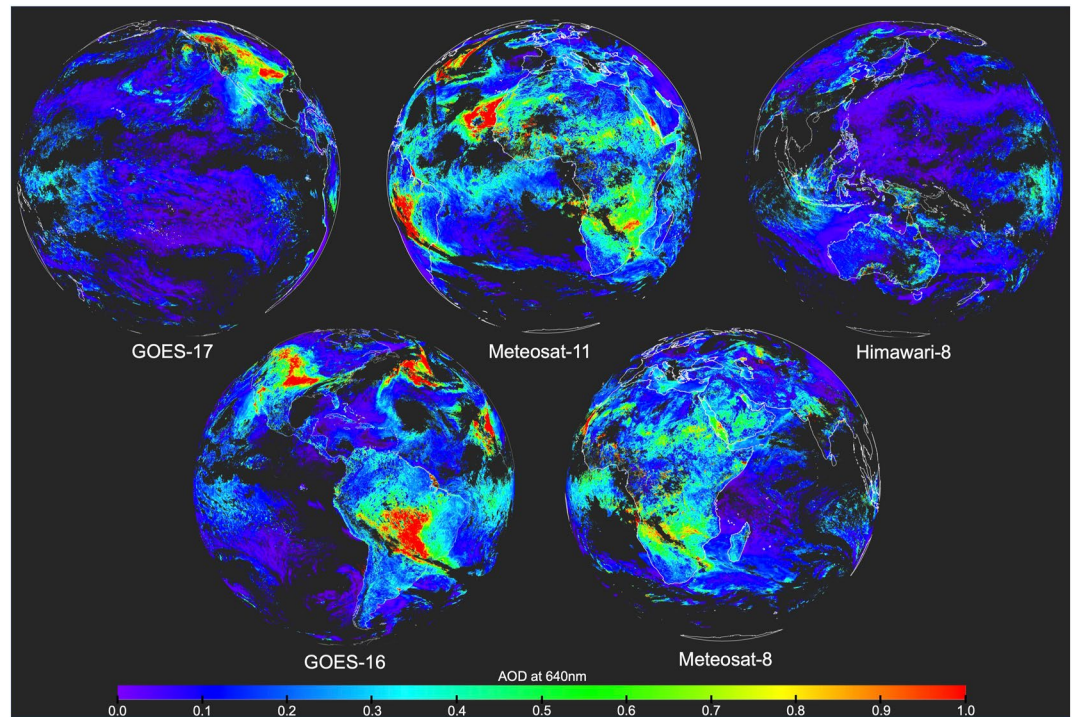


Figure 3. Maps of daily aerosol optical depth (AOD) at $0.64 \mu\text{m}$ on September 18, 2020, retrieved by AERUS-GEO from each of the five geostationary satellites.

obtained in previous studies. Indeed, Xu et al. (2014) found an average MBE of 0.02, a mean RMSE of 0.12, and a regression slope of 0.75 for the daily AOD retrieved from MSG. Similar scores were found by Carrer et al. (2010) over nine AERONET sites from June to September. It is important to emphasize that all AERONET stations with available retrievals were used for this investigation and that no selection of stations was done as it is often done in the literature. Furthermore, the use of AERONET Level 1.5 data could result in the use of some perfectible ground AOD inversions. The scores in Table 2 were obtained from a high number of AOD retrievals, which gives an average of 13 successful retrievals per station and per month (i.e., a monthly availability of 42.7%).

The quality of the AERUS-GEO aerosol retrievals is further assessed in Figure 4, which shows the spatial distribution of the error with respect to AERONET over the Earth's disk from each geostationary satellite. The average RMSE of each station was used to determine the color of the corresponding dot while the

Table 2
Quality Assessment of the Daily AOD Values Retrieved by AERUS-GEO From Each Geostationary Satellite

	GOES-17	GOES-16	Meteosat-11	Meteosat-8	Himawari-8	Total
r	0.80	0.73	0.80	0.73	0.69	0.76
MBE	0.01	0.01	0.02	0.01	0.01	0.01
RMSE	0.13	0.16	0.10	0.11	0.16	0.13
y	$0.96x - 0.00$	$0.88x + 0.01$	$0.74x + 0.02$	$0.69x + 0.04$	$0.70x + 0.05$	$0.80x + 0.02$
$\bar{\tau}_{\text{AERONET}}$	0.14	0.15	0.15	0.16	0.19	0.16
N (values)	7,332	10,173	10,462	9,557	3,468	40,992
n (stations)	139	166	193	195	94	787 ^a
Availability (%)	43.2	50.2	44.4	40.2	30.2	42.7

^aTotal number of stations does not take into account the fact that some sites are seen by several satellites at the same time.

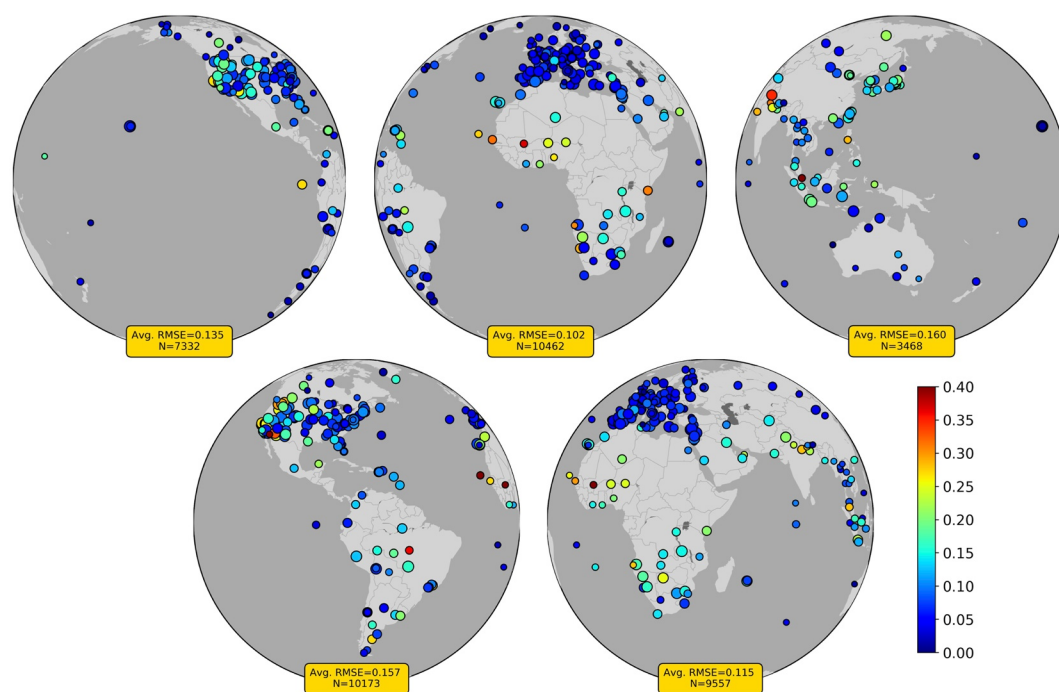


Figure 4. Maps showing the average root mean squared error (RMSE) for each Aerosol Robotic Network (AERONET) station considered for each geostationary satellite. The diameter of each dot is proportional to the number of samples.

diameter of each dot was set proportional to the number of coincident AOD retrievals. In general, RMSE values were found to be lower than 0.10 for most stations in Europe, the center and east of North America, Russia, South America, Southeast Asia, Oceania, and South Africa. Higher errors were found in the Amazonia and Northern and Central Africa due to the high aerosol concentrations that were recorded in these regions linked to intense dust and biomass burning events. The stations along the Indo-Gangetic Plain also obtained slightly degraded scores due to the high concentration of organic aerosols that is commonly found in this region (Singh et al., 2017). The higher errors found in Western US (and therefore for GOES-16 and GOES-17) were due to the exceptionally massive smoke aerosol plumes that were originated in the 2020 wildfire season (see Section 4.4 for more details). The average RMSE for Himawari-8 is slightly higher than for the rest of satellites due to the higher average AOD (see Table 2) coming from hazy regions in India, Japan, China, and Southeast Asia. Another reason may be the frequent cloudiness happening in the countries along the Equator (Singapore, Malaysia, and Indonesia), which makes more difficult the characterization of the surface BRDF.

4.3. Quasi-Global Maps of AOD

Individual maps of daily average AOD derived by AERUS-GEO from the five geostationary satellites were combined into a single quasi-global data set. This was done for each date from February to September, 2020, using the fusion method described in Section 3.2. The outcomes of this data processing are illustrated in Figure 5, which shows the quasi-global map retrieved for September 18, 2020 (see Figure 3 for the corresponding individual AOD maps). The daily AOD map does not show noteworthy artifacts nor discontinuities at the transitions between satellites. Estimates of aerosol load are available across the majority of the Earth thanks to the high coverage of the retrieved quasi-global map, which shows gaps for cloudy regions only.

The reasons behind the smoothness of the quasi-global AOD maps are threefold. First, AERUS-GEO provides reliable and smooth individual maps of AOD thanks to the robust disentangling of the aerosol signal and the spatial smoothing described in Section 2.2. Second, VIS06 channel is equivalent among all geostationary imagers (see Table 1), with a similar central wavelength around 640 nm. Differences in bandwidth are overcome by using coefficients specific to each spectral response function for (a) radiance-to-reflectance

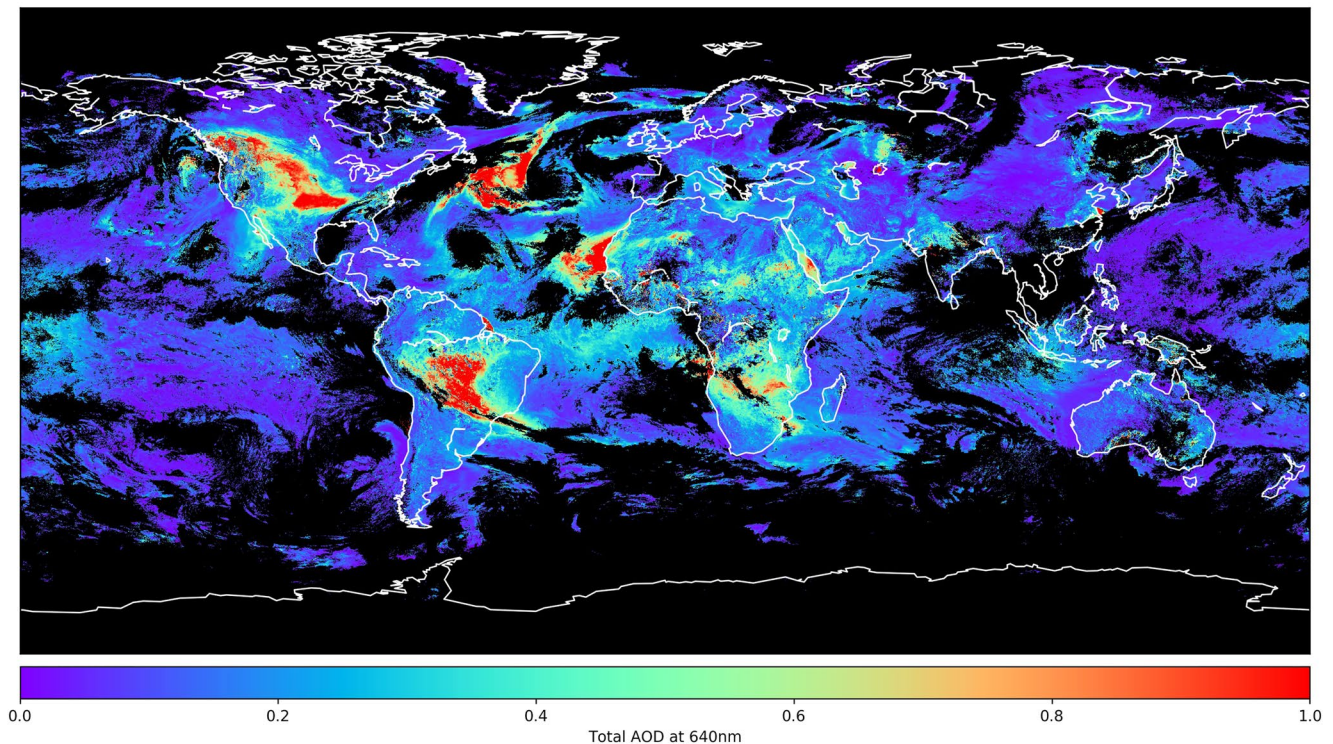


Figure 5. Quasi-global map of daily AOD at 640 nm on September 18, 2020, obtained by AERUS-GEO from the GEO-ring.

conversion and (b) molecular correction with SMAC. The lower SNR for SEVIRI is partly compensated by the debiasing procedure based on Meirink et al. (2013). Third, the dependence on $\cos \theta$, of the fusion weights allows smooth transitions among satellites.

4.3.1. Comparison to MODIS DT-DB Retrievals and CAMS Forecasts

Figure 6 shows the AOD jointly estimated from MODIS-Terra and MODIS-Aqua for September 18, 2020. The AOD maps from the two satellites were combined by simple averaging to increase the coverage of the DT-DB product for the comparison against AERUS-GEO. This combination was done despite the different overpass times of Terra and Aqua and the differences that were occasionally found between the AOD retrieved from the two satellites (Wei et al., 2019). These differences may be the reason behind the discontinuities observed in Figure 6 (e.g., over the Arabian Peninsula). Overall, the DT-DB and AERUS-GEO data sets were found to be highly correlated ($r = 0.79$), with the presence of remarkable aerosol plumes over North America, the Northern Atlantic Ocean, the Northwest coast of Africa, South America, and South Africa. The main difference between the two data sets is the lower spatial completeness of the DT-DB product with respect to AERUS-GEO. This mainly comes from the lower number of scans per day provided by polar orbiting satellites.

Figure 7 further illustrates the dissimilarity in geographical coverage between the two aerosol products by comparing the extent of the two satellite aerosol products for September 18, 2020, using a sinusoidal equal-area projection. According to Figure 7, the AERUS-GEO product covers 52.1% of the globe (combination of gold and salmon colors), which doubles the DT-DB products coverage with 26.2% of the globe (combination of blue and salmon colors). Areas exclusively covered by the AERUS-GEO product (pictured in gold color) represented 29.1% of the Earth and were found in many places around the world including regions with an intense aerosol activity. On the other hand, areas exclusively covered by the DT-DB products represent 3.2% of the planet only (pictured in blue color) and were mainly found in high latitudes where the coverage of geostationary satellites is limited.

The AERUS-GEO quasi-global AOD map in Figure 5 was also compared to Figure 8, which shows the total AOD at 670 nm forecasted by the near-real-time run of CAMS for September 18, 2020. The similarities

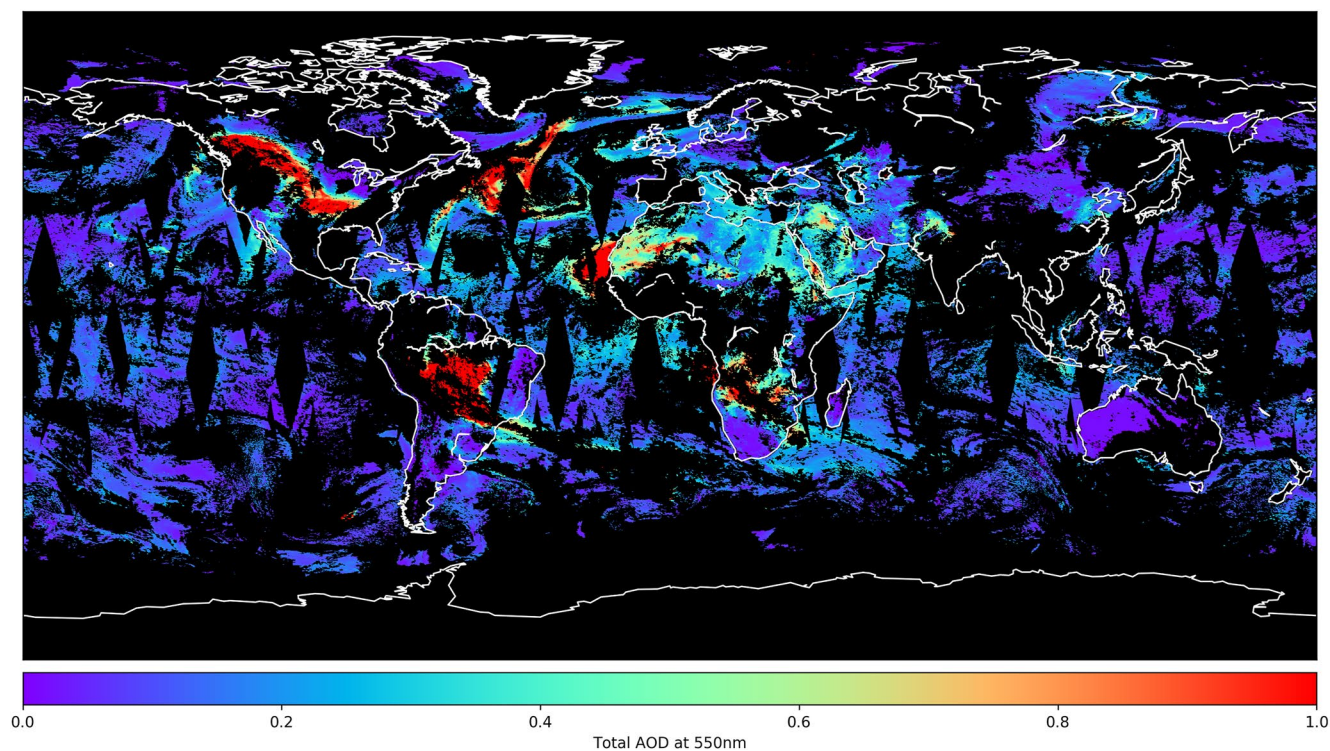


Figure 6. Global map of AOD at 550 nm on September 18, 2020, from the combined DT-DB aerosol products based on MODIS/Terra and MODIS/Aqua.

between AERUS-GEO, DT-DB, and CAMS data are obviously apparent, with noticeable aerosol plumes over similar regions. This cross-validation is more evident between CAMS and AERUS-GEO due to the highest coverage of the latter data set with respect to MODIS products. It is interesting to note the several

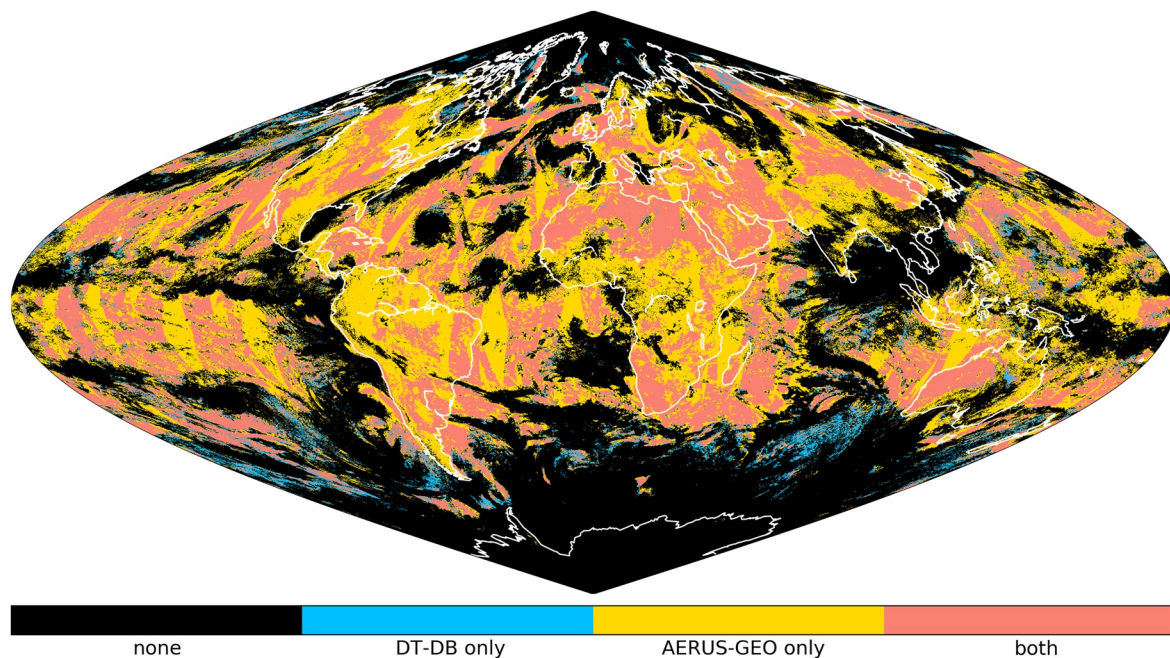


Figure 7. Geographical coverage of satellite aerosol products on September 18, 2020. Areas exclusively covered by the DT-DB products from Terra and Aqua appear in blue color, areas exclusively covered by the AERUS-GEO product appear in gold color, and areas covered by both products appear in salmon color. Areas not covered by any satellite product are in black color.

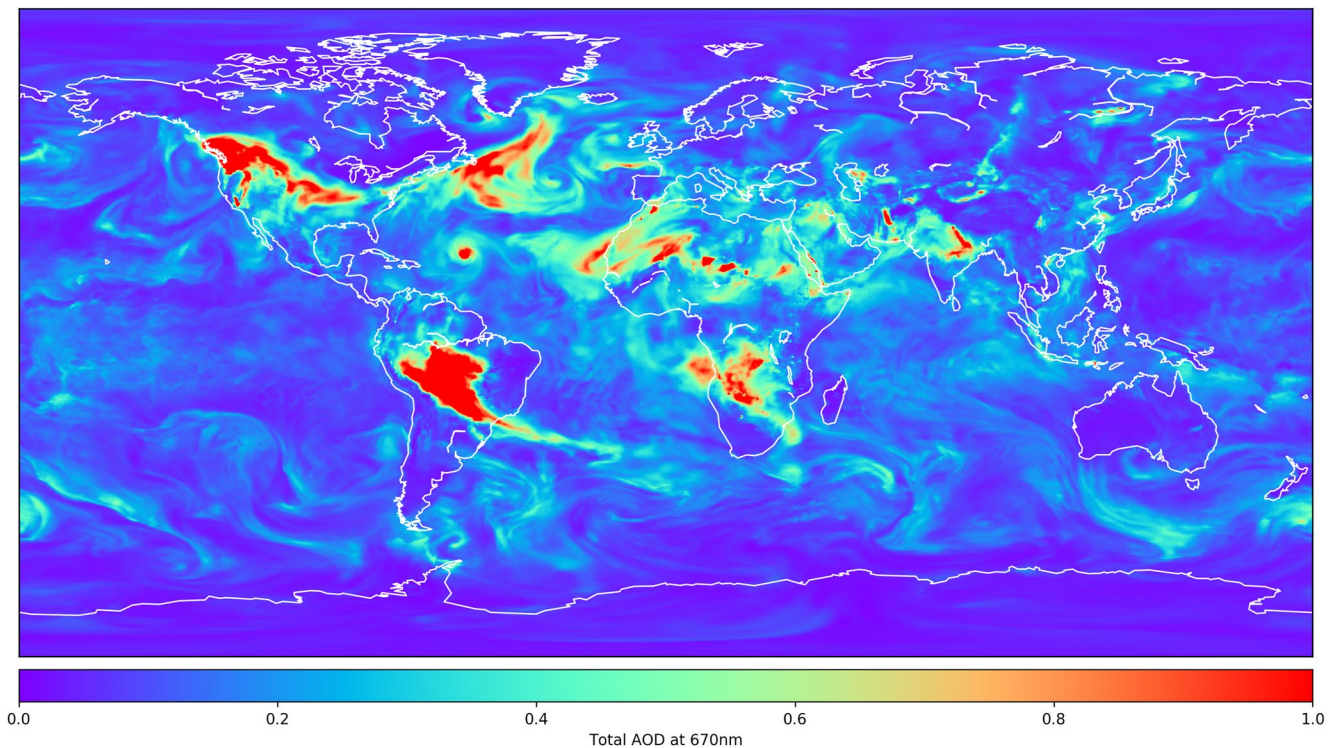


Figure 8. Global map of AOD at 670 nm on September 18, 2020, at noon forecasted by the Copernicus Atmosphere Monitoring Service (CAMS) near-real-time run.

differences existing between the model outputs and the satellite data sets such as the different shape and location of the aerosol plumes over North America or the different AOD magnitude over Afghanistan and Chad.

The three aerosol data sets are further compared in Figure 9 showing the correlation among maps of AOD from September 8 to 20, 2020. This period of time was marked by several large aerosol events including massive smoke plumes emitted from wildfires in America (see Section 4.4. for more details). Bias calculation among AOD maps was not possible due to the different wavelength among the three data sets. Correlation

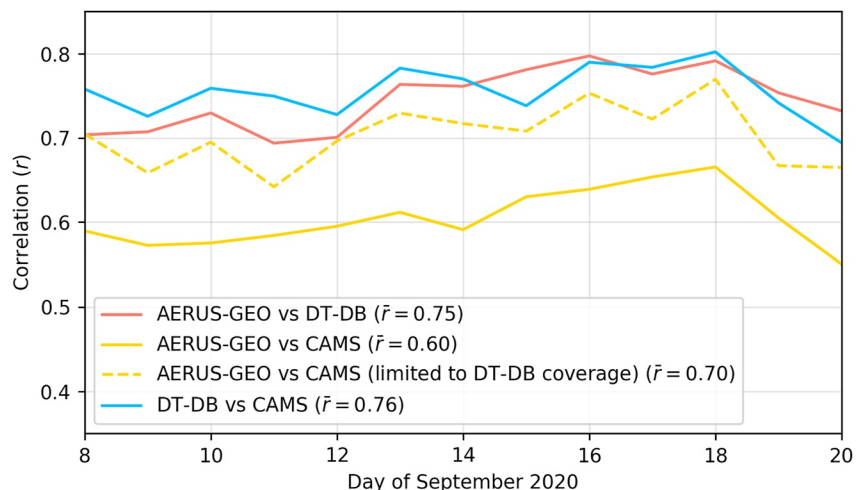


Figure 9. Temporal evolution of the correlation computed among AERUS-GEO, DT-DB, and CAMS maps of AOD from September 8 to 20, 2020.

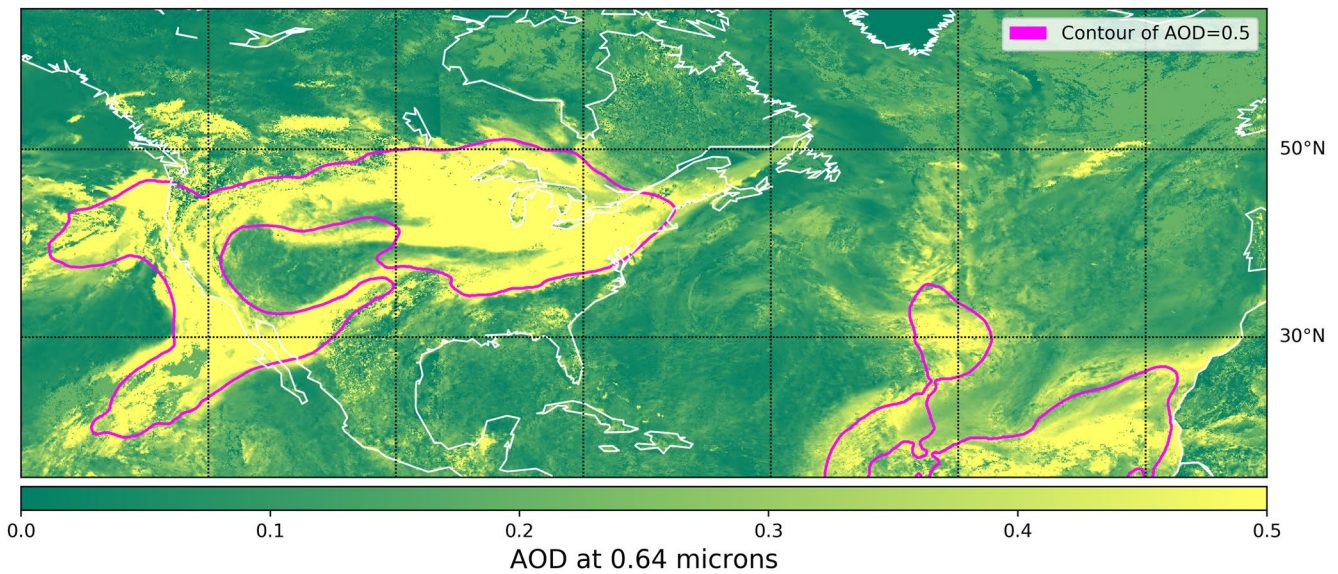


Figure 10. Daily AOD at 640 nm estimated by AERUS-GEO from the GEO-ring on September 14, 2020. The approximate contour of the aerosol plumes observed in the image when AOD is 0.5 is shown in pink. The massive smoke aerosol plumes coming from the 2020 Western US wildfires can be seen over North America.

was computed instead as this score is less impacted by this difference. Figure 9 shows a high correlation (average of 0.75) between AERUS-GEO and DT-DB aerosol data sets throughout the period of study. Similar scores obtained from the comparison between DT-DB and CAMS (average of 0.76) likely come from the assimilation of these MODIS aerosol data in the CAMS forecasting system. Correlation was found to be slightly lower between AERUS-GEO and CAMS data sets (average of 0.60). However, this score increased up to an average of 0.70 when the comparison was limited to the coverage of DT-DB (i.e., regions in salmon color in Figure 7). The lower agreement of AERUS-GEO with respect to CAMS over regions where DT-DB data were unavailable may be a sign of larger discrepancies between model and satellites due to the lack of assimilation. Similarly to the study done for Figure 7, the global coverage percentages averaged over the period of study were found to be 51.4% for AERUS-GEO and 26.6% for DT-DB, with 28.4% of pixels only contained in the GEO-ring based product and 3.6% of pixels only present in the MODIS-based product.

4.4. Monitoring Western United States Wildfire Smoke Aerosols in Summer 2020

The potential of the GEO-ring to monitor aerosols at the intercontinental scale is illustrated through the case study of the Western US wildfires in 2020. Fires originated mostly in the states of California, Oregon, and Washington and emitted large amounts of smoke and pollutants. The wildfire season in 2020 was the largest recorded in California's modern history according to the California Department of Forestry and Fire Protection with the burning of 4% of the state (1,690,718 ha) due to the 9,639 recorded fires (<https://www.fire.ca.gov/incidents/2020/>). High concentration of particles emitted from these prolonged wildfires stayed in the atmosphere for days with an intense intercontinental transport over thousands of kilometers across the Atlantic Ocean. Two episodes of long-range-transported aerosols were observed from space, the first in the second half of August and the second during the first half of September.

The quasi-global daily AOD maps provided by AERUS-GEO were used in this investigation to monitor the smoke aerosol plumes originated in the Western US wildfires. Figure 10 shows the part of the map derived on September 14, 2020, encompassing North America and the Northern Atlantic Ocean. A massive aerosol plume with high values of AOD is observed for this date, extending from the Northeastern Pacific Ocean to the East of the US and from North West Mexico to South East Canada. Dust aerosols are also observed along the West Coast of Africa. The absence of gaps in Figure 10 is achieved for the sake of visualization by filling the missing values with the latest available daily AOD retrieval. The approximate contour of the

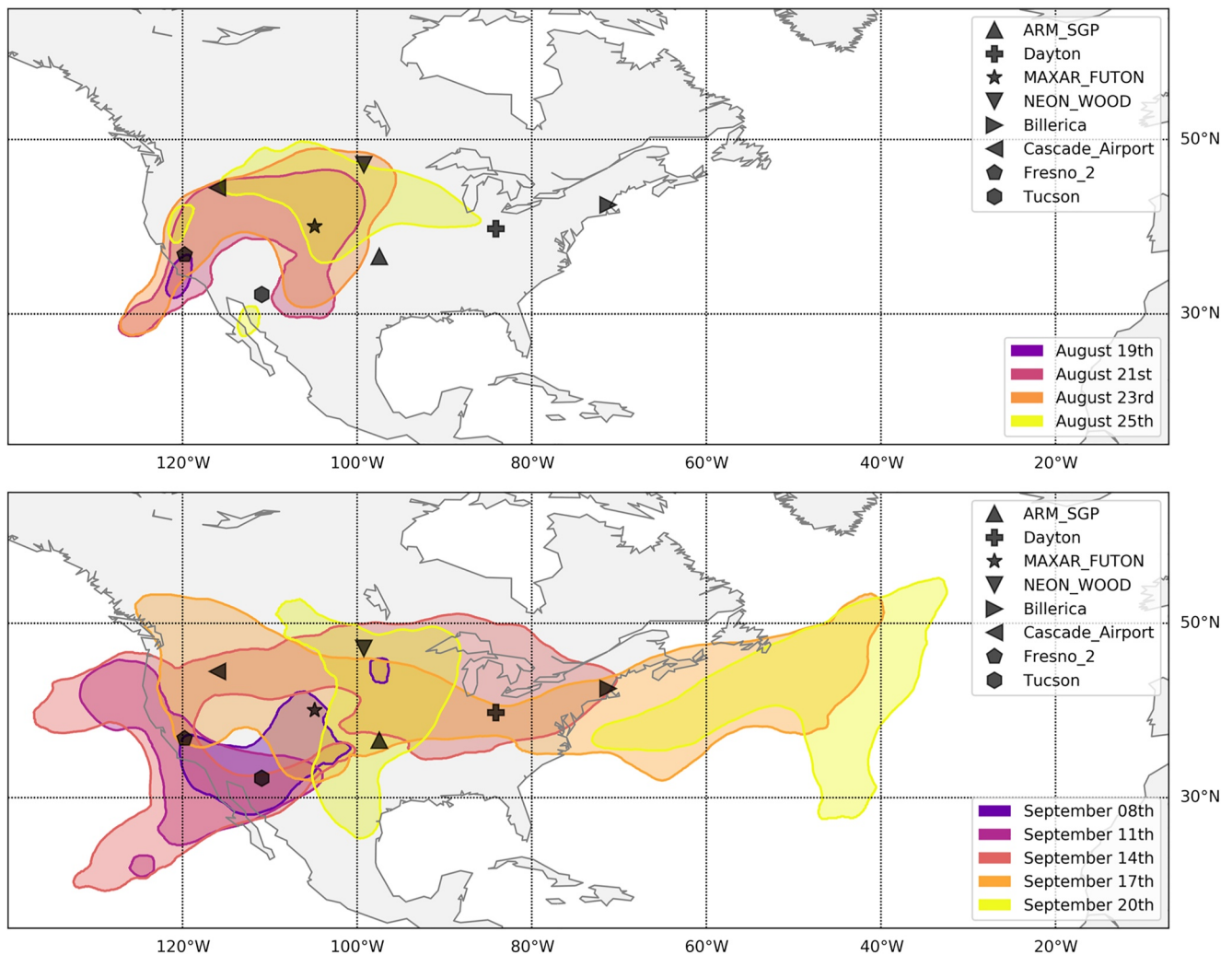


Figure 11. Transport of smoke aerosols from Western US wildfires in August (top) and September (bottom) 2020, observed by AERUS-GEO. Colored layers indicate the extent of the smoke plume when AOD at $0.64 \mu\text{m}$ was equal to or greater than 0.5.

aerosol plumes when AOD at 640 nm is 0.5 is shown in pink. Contours were extracted by standard image processing.

The contours of the aerosol plume when AOD equals 0.5 were extracted for each day of the two episodes of long-range transport of aerosol particles in August and September. Figure 11(top) shows the transport of the smoke plumes originated in Western US by plotting the contours for August 19, 21, 23, and 25 in different colors. During this first episode, smoke aerosols traveled from California to the northeast until Chicago, in the Midwestern US, on August 25. The aerosol plume also traveled to the south getting to the states of Colorado and New Mexico on August 21. Figure 11(bottom) shows a transport of smoke particles over longer distances for the second episode from September 8 to 20. In this case, high concentrations of smoke particles were found over the most part of the US, Northern Mexico, and Southern Canada before reaching the Atlantic Ocean on September 20. One reason behind this long-range transport was the development of a rare pyrocumulonimbus in Southern California which projected at higher altitudes the fire-emitted materials, such as gas and particles (<https://www.nasa.gov/feature/goddard/2020/californias-creek-fire-creates-its-own-pyrocumulonimbus-cloud>). Vertical uplift plays a role in spreading fire emissions over longer distances, due to the fact that horizontal transport is more efficient at a higher altitude in the atmosphere because of stronger winds and therefore, removal of these products is less efficient (Fromm et al., 2008). As can be seen, the aerosol maps derived by AERUS-GEO from the GEO-ring provided valuable data for the

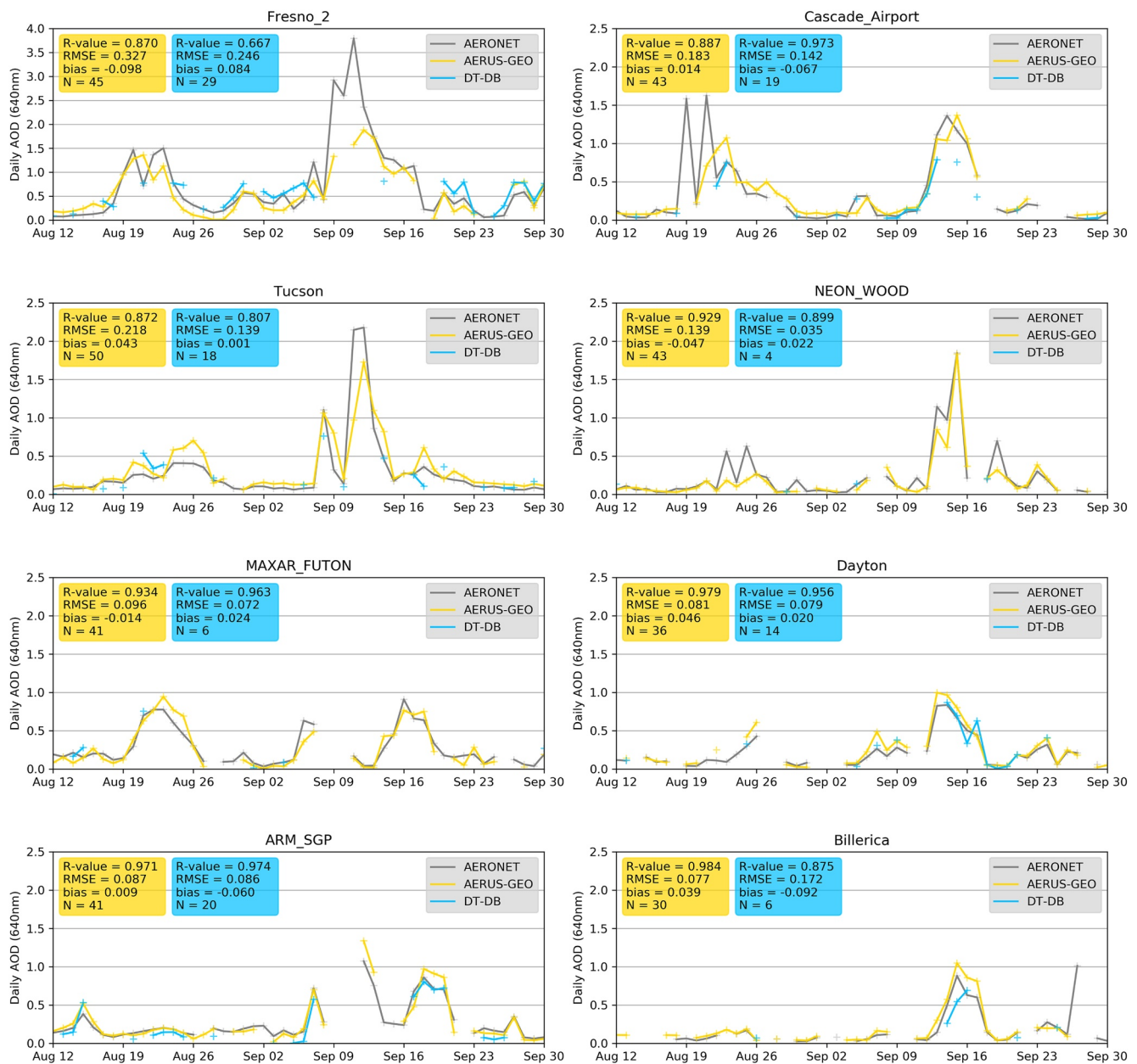


Figure 12. Time series of daily AOD from AERUS-GEO and DT-DB aerosol products over eight AERONET stations during the long-range transport of smoke and pollutants emitted by the Western US wildfires in 2020.

monitoring of the long-range-transported aerosol plumes of the selected case study, with the simultaneous use of up to four geostationary satellites for the second episode in September (i.e., GOES-17, GOES-16, Meteosat-11, and Meteosat-8).

The accuracy of the AERUS-GEO retrievals during the 2020 Western US wildfires was assessed by inspecting their temporal evolution compared to AERONET daily retrievals. Figure 11 shows the daily AOD estimated by AERUS-GEO and AERONET between August 12 and September 30 for eight stations scattered over the US (see Figure 11 for their location). AOD provided by the MODIS-based DT-DB product was also plotted for comparison after conversion to 640 nm using AERONET spectral measurements. Taking a closer look at the second episode in September, Figure 12 shows how high concentrations of smoke aerosols were injected into the atmosphere starting on September 9 in Western US (see Fresno_2 station with AOD values up to 3.7), then transported through two different branches on 12 and 13 (one in the north, see Cascade_Airport

station, and another in the south, see Tucson station), across the Midwest on 14 (see Dayton stations), until reaching the Northeastern US on 15 (see Billerica station with AOD values close to 1). Overall, the AERUS-GEO daily AOD inversions shown in Figure 12 match the AERONET inversions with high correlation and low errors, which are similar to those obtained by DT-DB retrievals. However, MODIS-based time series of AOD show a significantly lower number of retrievals (116 successful retrievals over all stations compared to 329 for AERUS-GEO), which result in the missing of some peaks of aerosol concentration (e.g., September 10 and 11 over Tucson and NEON-WOOD stations).

5. Discussion

This article illustrates and demonstrates the potential for aerosol monitoring of a ring of geostationary meteorological satellites combined with appropriate retrieval algorithms. In this investigation, data provided by the imagers aboard the satellites GOES-17, GOES-16, Meteosat-11, Meteosat-8, and Himawari-8 were processed by the algorithm AERUS-GEO to provide quasi-global maps of total AOD. These aerosol data were found to be accurate, smooth, and complete in part due to the high number of full-disk scans per day provided by geostationary imagers. This advantage of the GEO-ring allowed AERUS-GEO to retrieve AOD for 51.4% of the Earth for a given date, whereas the combined DT-DB aerosol products derived from MODIS-Terra and MODIS-Aqua reached a coverage of 26.6%. The different number of Earth views per day between geostationary and polar orbiting satellites lead to aerosol products for which 28.4% of the globe is exclusively covered by AERUS-GEO. A high temporal completeness was also found for AERUS-GEO retrievals, with an AOD estimate for 42.7% of the days (the majority of the rest being cloudy during most part of the day). The accuracy of these aerosol retrievals was validated based on the agreement with AERONET measurements and the correlation with DT-DB AOD maps. These results demonstrate the great value of aerosol data derived from a constellation of geostationary imagers to, for example, improve aerosol forecasting through data assimilation. Global atmospheric models may indeed benefit from the completeness of the AERUS-GEO retrievals obtained from the GEO-ring. In the case of CAMS, some differences were observed between the forecasted AOD values and the AERUS-GEO product despite the generally high correlation between the two data sets. These differences, which were mainly observed in regions unseen in the DT-DB product but covered by AERUS-GEO, prove the potential benefits of assimilating GEO-ring derived aerosol data to improve CAMS forecasts. Nowadays, the CAMS near-real time system exclusively assimilates aerosol products coming from polar orbiting satellites including MODIS DT and DB (Rémy et al., 2019). In addition to the benefits for aerosol forecasting, this investigation proved the utility of the aerosol data derived from the GEO-ring to study long-range-transported aerosols such as the Western US wildfire smoke episode in 2020. For this particular event, AERUS-GEO was reported to provide 3 times more AOD retrievals than the DT-DB product.

The quasi-global AOD retrievals presented in this work could be improved if some pending limitations of the AERUS-GEO algorithm were overcome. This includes the consideration of a single continental aerosol type and the use of a Lambertian BRDF for oceans. Albeit AERUS-GEO was optimized to minimize the impact of these assumptions, potentially significant errors could be occasionally introduced in the retrieved AOD values for some particular cases (e.g., intense aerosol activity and retrievals over bright surfaces). The improvement of these limitations is currently being addressed in a novel version of the AERUS-GEO algorithm that is under development (Ceamanos, Moparthy, Carrer, & Six, 2019). The new method, which is named i-AERUS-GEO, will include the use of (a) several aerosol models described by accurate optical properties to cover the large variety of aerosol particles, (b) an appropriate BRDF model for ocean surfaces taking into account the directional properties of water reflectance, (c) spatial and temporal homogeneity constraints to improve the AOD inversion, and (d) a more accurate RTM. Furthermore, i-AERUS-GEO will exploit the full capacity of SEVIRI in terms of temporal resolution with the retrieval of AOD every 15 min. This work will join the efforts that are currently underway to retrieve the diurnal evolution of aerosol properties from geostationary missions such as MSG (Luffarelli & Govaerts, 2019), Himawari (Gupta et al., 2019; Lyapustin et al., 2019; Yoshida et al., 2018), GOES (Zhang et al., 2020), and GOCI (Lennartson et al., 2018). Information on subdaily AOD variations is key in many studies such as the calculation of aerosol radiative forcing (Xu et al., 2016). The combination of diurnal AOD retrievals and quasi-global coverage that can be made possible by the GEO-ring will certainly be of great interest to the aerosol community. Future work

will also investigate further the fusion strategy among geostationary satellites to optimize the quality of the AOD retrievals in the overlapping regions.

6. Conclusions

Geostationary meteorological satellites are recently receiving a great deal of attention from the aerosol remote sensing community due to their unprecedented performances for continuous aerosol monitoring. However, the main shortcoming of this type of satellites is the limitation of their spatial coverage to the Earth's disk that is observed from the geostationary orbit. The simultaneous use of five geostationary satellites evenly spaced around the planet was used in this article to overcome this limitation. Quasi-global maps of total AOD were provided from the so-called GEO-ring formed by the operational geostationary weather satellites GOES-17, GOES-16, Meteosat-11, Meteosat-8, and Himawari-8. The retrieval algorithm AERUS-GEO was used to provide estimates of daily-averaged AOD from each satellite before combining them into a single global map. The spatiotemporal completeness of the resulting quasi-global AOD maps produced in this study was found to be higher (2 times more spatial coverage and 3 times more temporal coverage) with respect to the aerosol products derived from MODIS aboard the polar orbiting satellites Terra and Aqua due to the multiple views per day of geostationary satellites. Comparison to ground measurements from the AERONET network confirmed the accuracy of the GEO-ring based AOD retrievals, with an average correlation, MBE, and RMSE of 0.76, 0.01, and 0.13, respectively. The strong potential for aerosol studies of the resulting quasi-global maps of daily AOD was illustrated by focusing on the long-range transport of aerosol particles from the Western US wildfires to the Atlantic Ocean. Furthermore, the accuracy, smoothness, and completeness of the aerosol data provided by AERUS-GEO from the GEO-ring were found to be of great value to improve global atmospheric models such as CAMS through data assimilation.

To the best of our knowledge, this investigation is pioneering in illustrating and assessing the potential of a GEO-ring of meteorological satellites for the study of aerosols. Furthermore, this study is a prelude of the unprecedented monitoring of aerosols at high temporal resolution and high precision that will become possible when the Meteosat Third Generation-Imager (MTG-I) satellites will be in orbit (Holmlund et al., 2021). The next generation of EUMETSAT geostationary weather satellites will be equipped with the Flexible Combined Imager (FCI), which will be comparable to ABI on GOES-16/17 and AHI on Himawari-8 in terms of spatial, spectral, and temporal performances. MTG-I will complete a GEO-ring of imagers of next generation that should improve the aerosol retrievals presented in this study, which are in part limited by the reduced spectral range of the SEVIRI instrument with respect to AHI and ABI. In particular, improvements are expected on aerosol retrieval thanks to the new FCI spectral bands in the blue and 2.1 μm wavelengths, which are used in MODIS aerosol retrievals for example (Lyapustin et al., 2018).

Data Availability Statement

The maps of daily AOD that were used in this investigation can be accessed through the following link upon free registration on the ICARE Data and Service Center: https://www.icare.univ-lille.fr/data-access/data-archive-access/?dir=PUBLICATION_DATA/10.1029/2021JD034906/.

References

- Benedetti, A., Morcrette, J.-J., Boucher, O., Dethof, A., Engelen, R., Fisher, M., et al. (2009). Aerosol analysis and forecast in the European Centre for Medium-Range Weather Forecasts Integrated Forecast System: 2. Data assimilation. *Journal of Geophysical Research*, *114*, D13205. <https://doi.org/10.1029/2008JD011115>
- Bernard, E., Moulin, C., Ramon, D., Jolivet, D., Riedi, J., & Nicolas, J.-M. (2011). Description and validation of an AOT product over land at the 0.6 μm channel of the SEVIRI sensor onboard MSG. *Atmospheric Measurement Techniques*, *4*, 2543–2565. <https://doi.org/10.5194/amt-4-2543-2011>
- Bessho, K., Date, K., Hayashi, M., Ikeda, A., Imai, T., Inoue, H., et al. (2016). An introduction to Himawari-8/9—Japan's new-generation geostationary meteorological satellites. *Journal of the Meteorological Society of Japan*, *94*, 151–183. <https://doi.org/10.2151/jmsj.2016-009>
- Boucher, O., Randall, D., Artaxo, P., Bretherton, C., Feingold, G., Forster, P., et al. (2013). Clouds and aerosols. In T. F. Stocker, et al. (Eds.), *Climate change 2013: The physical science basis. Contribution of Working Group I to the Fifth Assessment Report of the Intergovernmental Panel on Climate Change*. Cambridge University Press.
- Carrer, D., Ceamanos, X., Six, B., & Roujean, J.-L. (2014). AERUS-GEO: A newly available satellite-derived aerosol optical depth product over Europe and Africa. *Geophysical Research Letters*, *41*, 7731–7738. <https://doi.org/10.1002/2014GL061707>

Acknowledgments

The authors thank Dominique Carrer for sharing his knowledge on AERUS-GEO. Suman Moparthy is acknowledged for his contribution to the development of the validation tools. The authors also thank the investigators and their staff for establishing and maintaining the AERONET sites used in this investigation. The French space agency CNES is acknowledged for providing the SMAC coefficients that were used to process the different geostationary satellites. Jan Fokke Meirink from KNMI is thanked for sharing his latest findings on SEVIRI calibration. The SATMOS/CMS center is acknowledged for providing the satellite radiances and cloud masks for the five geostationary satellites.

- Carrer, D., Moparth, S., Lellouch, G., Ceamanos, X., Pinault, F., Freitas, S. C., & Trigo, I. F. (2018). Land surface albedo derived on a ten daily basis from Meteosat Second Generation Observations: The NRT and climate data record collections from the EUMETSAT LSA SAF. *Remote Sensing*, *10*(8), 1262. <https://doi.org/10.3390/rs10081262>
- Carrer, D., Roujean, J.-L., Hauteceur, O., & Elias, T. (2010). Daily estimates of aerosol optical thickness over land surface based on a directional and temporal analysis of SEVIRI MSG visible observations. *Journal of Geophysical Research*, *115*, D10208. <https://doi.org/10.1029/2009JD012272>
- Ceamanos, X., Carrer, D., & Roujean, J.-L. (2014). Improved retrieval of direct and diffuse downwelling surface shortwave flux in cloudless atmosphere using dynamic estimates of aerosol content and type: Application to the LSA-SAF project. *Atmospheric Chemistry and Physics*, *14*, 8209–8232. <https://doi.org/10.5194/acp-14-8209-2014>
- Ceamanos, X., Moparth, S., Carrer, D., & Seidel, F. C. (2019). Assessing the potential of geostationary satellites for aerosol remote sensing based on critical surface albedo. *Remote Sensing*, *11*, 2958. <https://doi.org/10.3390/rs11242958>
- Ceamanos, X., Moparth, S., Carrer, D., & Six, B. (2019). Retrieving the diurnal cycle of aerosol optical depth from current and future Meteosat geostationary satellites. *Paper presented at American Geophysical Union Fall Meeting, San Francisco, CA.*
- Choi, M., Kim, J., Lee, J., Kim, M., Park, Y.-J., Jeong, U., et al. (2016). GOCI Yonsei Aerosol Retrieval (YAER) algorithm and validation during the DRAGON-NE Asia 2012 campaign. *Atmospheric Measurement Techniques*, *9*, 1377–1398. <https://doi.org/10.5194/amt-9-1377-2016>
- Derrien, M., & Le Gleau, H. (2005). MSG/SEVIRI cloud mask and type from SAFNWC. *International Journal of Remote Sensing*, *26*, 4707–4732. <https://doi.org/10.1080/01431160500166128>
- Escribano, J., Boucher, O., Chevallier, F., & Huneeus, N. (2017). Impact of the choice of the satellite aerosol optical depth product in a sub-regional dust emission inversion. *Atmospheric Chemistry and Physics*, *17*, 7111–7126. <https://doi.org/10.5194/acp-17-7111-2017>
- Fromm, M., Shettle, E. P., Fricke, K. H., Ritter, C., Trickl, T., Giehler, H., et al. (2008). Stratospheric impact of the Chisholm pyrocumulonimbus eruption: 2. Vertical profile perspective. *Journal of Geophysical Research*, *113*, D08203. <https://doi.org/10.1029/2007JD009147>
- Giles, D. M., Sinyuk, A., Sorokin, M. G., Schafer, J. S., Smirnov, A., Slutsker, I., et al. (2019). Advancements in the Aerosol Robotic Network (AERONET) Version 3 database—Automated near-real-time quality control algorithm with improved cloud screening for Sun photometer aerosol optical depth (AOD) measurements. *Atmospheric Measurement Techniques*, *12*, 169–209. <https://doi.org/10.5194/amt-12-169-2019>
- Gomez-Amo, J. L., Estelles, V., Marcos, C., Segura, S., Esteve, A. R., Pedros, R., et al. (2017). Impact of dust and smoke mixing on column-integrated aerosol properties from observations during a severe wildfire episode over Valencia (Spain). *The Science of the Total Environment*, *599–600*, 2121–2134. <https://doi.org/10.1016/j.scitotenv.2017.05.041>
- Govaerts, Y. M., Wagner, S., Lattanzio, A., & Watts, P. (2010). Joint retrieval of surface reflectance and aerosol optical depth from MSG/SEVIRI observations with an optimal estimation approach: 1. Theory. *Journal of Geophysical Research*, *115*, D02203. <https://doi.org/10.1029/2009JD011779>
- Gupta, P., Levy, R. C., Mattoo, S., Remer, L. A., Holz, R. E., & Heidinger, A. K. (2019). Applying the Dark Target aerosol algorithm with Advanced Himawari Imager observations during the KORUS-AQ field campaign. *Atmospheric Measurement Techniques*, *12*, 6557–6577. <https://doi.org/10.5194/amt-12-6557-2019>
- Holben, B. N., Eck, T. F., Slutsker, I., Tanré, D., Buis, J. P., Setzer, A., et al. (1998). AERONET—A federated international network and data archive for aerosol characterization. *Remote Sensing of Environment*, *66*, 1–16. [https://doi.org/10.1016/S0034-4257\(98\)00031-5](https://doi.org/10.1016/S0034-4257(98)00031-5)
- Holmlund, K., Grandell, J., Schmetz, J., Stuhlmann, R., Bojkov, B., Munro, R., et al. (2021). Meteosat Third Generation (MTG): Continuation and innovation of observations from geostationary orbit. *Bulletin of the American Meteorological Society*, *102*(5), E990–E1015. <https://doi.org/10.1175/BAMS-D-19-0304.1>
- Hsu, N. C., Jeong, M.-J., Bettenhausen, C., Sayer, A. M., Hansell, R., Seftor, C. S., et al. (2013). Enhanced Deep Blue aerosol retrieval algorithm: The second generation. *Journal of Geophysical Research: Atmospheres*, *118*, 9296–9315. <https://doi.org/10.1002/jgrd.50712>
- Hu, Q., Goloub, P., Veselovskii, I., Bravo-Aranda, J.-A., Popovici, I. E., Podvin, T., et al. (2019). Long-range-transported Canadian smoke plumes in the lower stratosphere over northern France. *Atmospheric Chemistry and Physics*, *19*, 1173–1193. <https://doi.org/10.5194/acp-19-1173-2019>
- Knapp, K. R. (2002). Quantification of aerosol signal in GOES 8 visible imagery over the United States. *Journal of Geophysical Research*, *107*(D20), 4426. <https://doi.org/10.1029/2001JD002001>
- Kondragunta, S., Laszlo, I., Zhang, H., Ciren, P., & Huff, A. (2020). Air quality applications of ABI aerosol products from the GOES-R series. In *The GOES-R series: A new generation of geostationary environmental satellites* (pp. 203–217). Elsevier. <https://doi.org/10.1016/B978-0-12-814327-8.00017-2>
- Kotchenova, S. Y., Vermote, E. F., Matarrese, R., & Klemm, F. J., Jr. (2006). Validation of a vector version of the 6S radiative transfer code for atmospheric correction of satellite data. Part I: Path radiance. *Applied Optics*, *45*(26), 6762–6774. <https://doi.org/10.1364/AO.45.006762>
- Lennartson, E. M., Wang, J., Gu, J., Castro Garcia, L., Ge, C., Gao, M., et al. (2018). Diurnal variation of aerosol optical depth and PM_{2.5} in South Korea: A synthesis from AERONET, satellite (GOCI), KORUS-AQ observation, and the WRF-Chem model. *Atmospheric Chemistry and Physics*, *18*, 15125–15144. <https://doi.org/10.5194/acp-18-15125-2018>
- Levy, R. C., Mattoo, S., Munchak, L. A., Remer, L. A., Sayer, A. M., Patadia, F., & Hsu, N. C. (2013). The Collection 6 MODIS aerosol products over land and ocean. *Atmospheric Measurement Techniques*, *6*, 2989–3034. <https://doi.org/10.5194/amt-6-2989-2013>
- Lim, H., Choi, M., Kim, J., Kasai, Y., & Chan, P. W. (2018). AHI/Himawari-8 Yonsei Aerosol Retrieval (YAER): Algorithm, validation and merged products. *Remote Sensing*, *10*, 699. <https://doi.org/10.3390/rs10050699>
- Lim, H., Go, S., Kim, J., Choi, M., Lee, S., Song, C.-K., & Kasai, Y. (2021). Integration of GOCI and AHI Yonsei aerosol optical depth products during the 2016 KORUS-AQ and 2018 EMERG campaigns. *Atmospheric Measurement Techniques*, *14*, 4575–4592. <https://doi.org/10.5194/amt-14-4575-2021>
- Lucht, W., Schaaf, C. B., & Strahler, A. H. (2000). An algorithm for the retrieval of albedo from space using semiempirical BRDF models. *IEEE Transactions on Geoscience and Remote Sensing*, *38*, 977–998. <https://doi.org/10.1109/36.841980>
- Luffarelli, M., & Govaerts, Y. (2019). Joint retrieval of surface reflectance and aerosol properties with continuous variation of the state variables in the solution space—Part 2: Application to geostationary and polar-orbiting satellite observations. *Atmospheric Measurement Techniques*, *12*, 791–809. <https://doi.org/10.5194/amt-12-791-2019>
- Lyapustin, A., Wang, Y., Korkin, S., & Huang, D. (2018). MODIS Collection 6 MAIAC algorithm. *Atmospheric Measurement Techniques*, *11*, 5741–5765. <https://doi.org/10.5194/amt-11-5741-2018>
- Lyapustin, A., Wang, Y., Korkin, S., Nemani, R. R., & Wang, W. (2019). High-resolution aerosol retrievals from geostationary observations with algorithm MAIAC. *Paper presented at American Geophysical Union Fall Meeting, San Francisco, CA.*
- Meirink, J. F., Roebeling, R. A., & Stammes, P. (2013). Inter-calibration of polar imager solar channels using SEVIRI. *Atmospheric Measurement Techniques*, *6*, 2495–2508. <https://doi.org/10.5194/amt-6-2495-2013>

- Morcrette, J.-J., Boucher, O., Jones, L., Salmond, D., Bechtold, P., Beljaars, A., et al. (2009). Aerosol analysis and forecasting the European Centre for Medium-Range Weather Forecasts Integrated Forecast System: Forward modeling. *Journal of Geophysical Research*, *114*, D06206. <https://doi.org/10.1029/2008JD011235>
- Nabat, P., Somot, S., Mallet, M., Michou, M., Sevault, F., Driouech, F., et al. (2015). Dust aerosol radiative effects during summer 2012 simulated with a coupled regional aerosol-atmosphere-ocean model over the Mediterranean. *Atmospheric Chemistry and Physics*, *15*, 3303–3326. <https://doi.org/10.5194/acp-15-3303-2015>
- Popp, T., De Leeuw, G., Bingen, C., Brühl, C., Capelle, V., Chedin, A., et al. (2016). Development, production and evaluation of aerosol climate data records from European satellite observations (Aerosol_cci). *Remote Sensing*, *8*, 421. <https://doi.org/10.3390/rs8050421>
- Rahman, H., & Dedieu, G. (1994). SMAC: A simplified method for the atmospheric correction of satellite measurements in the solar spectrum. *International Journal of Remote Sensing*, *15*(1), 123–143. <https://doi.org/10.1080/01431169408954055>
- Remer, L. A., Levy, R. C., Mattoo, S., Tanré, D., Gupta, P., Shi, Y., et al. (2020). The Dark Target algorithm for observing the global aerosol system: Past, present, and future. *Remote Sensing*, *12*, 2900. <https://doi.org/10.3390/rs12182900>
- Rémy, S., Kipling, Z., Flemming, J., Boucher, O., Nabat, P., Michou, M., et al. (2019). Description and evaluation of the tropospheric aerosol scheme in the European Centre for Medium-Range Weather Forecasts (ECMWF) Integrated Forecasting System (IFS-AER, cycle 45R1). *Geoscientific Model Development*, *12*, 4627–4659. <https://doi.org/10.5194/gmd-12-4627-2019>
- Roberts, A. J., Woodage, M. J., Marsham, J. H., Highwood, E. J., Ryder, C. L., McGinty, W., et al. (2018). Can explicit convection improve modelled dust in summertime West Africa? *Atmospheric Chemistry and Physics*, *18*, 9025–9048. <https://doi.org/10.5194/acp-18-9025-2018>
- Schmetz, J., Pili, P., Tjemkes, S., Just, D., Kerkmann, J., Rota, S., & Ratier, A. (2002). An introduction to Meteosat Second Generation (MSG). *Bulletin of the American Meteorological Society*, *83*, 977–992. [https://doi.org/10.1175/1520-0477\(2002\)083<0992:STAITM>2.3.CO;2](https://doi.org/10.1175/1520-0477(2002)083<0992:STAITM>2.3.CO;2)
- Schmit, T. J., Griffith, P., Gunshor, M. M., Daniels, J. M., Goodman, S. J., & Lebar, W. J. (2017). A closer look at the ABI on the GOES-R series. *Bulletin of the American Meteorological Society*, *98*(4), 681–698. <https://doi.org/10.1175/BAMS-D-15-00230.1>
- Singh, N., Mhawish, A., Deboudt, K., Singh, R. S., & Banerjee, T. (2017). Organic aerosols over Indo-Gangetic Plain: Sources, distributions and climatic implications. *Atmospheric Environment*, *157*, 59–74. <https://doi.org/10.1016/j.atmosenv.2017.03.008>
- Stevens, B., & Feingold, G. (2009). Untangling aerosol effects on clouds and precipitation in a buffered system. *Nature*, *461*(7264), 607–613. <https://doi.org/10.1038/nature08281>
- Thieuleux, F., Moulin, C., Bréon, F. M., Maignan, F., Poitou, J., & Tanré, D. (2005). Remote sensing of aerosols over the oceans using MSG/SEVIRI imagery. *Annales Geophysicae*, *23*, 3561–3568. <https://doi.org/10.5194/angeo-23-3561-2005>
- Wei, J., Peng, Y., Guo, J., & Sun, L. (2019). Performance of MODIS Collection 6.1 Level 3 aerosol products in spatial-temporal variations over land. *Atmospheric Environment*, *206*, 30–44. <https://doi.org/10.1016/j.atmosenv.2019.03.001>
- Wei, X., Chang, N.-B., Bai, K., & Gao, W. (2020). Satellite remote sensing of aerosol optical depth: Advances, challenges, and perspectives. *Critical Reviews in Environmental Science and Technology*, *50*(16), 1640–1725. <https://doi.org/10.1080/10643389.2019.1665944>
- Xie, Y., Xue, Y., Guang, J., Mei, L., She, L., Li, Y., et al. (2020). Deriving a global and hourly data set of aerosol optical depth over land using data from four geostationary satellites: GOES-16, MSG-1, MSG-4, and Himawari-8. *IEEE Transactions on Geoscience and Remote Sensing*, *58*(3), 1538–1549. <https://doi.org/10.1109/TGRS.2019.2944949>
- Xu, H., Ceamanos, X., Roujean, J.-L., Carrer, D., & Xue, Y. (2014). Can satellite-derived aerosol optical depth quantify the surface aerosol radiative forcing? *Atmospheric Research*, *150*, 151–167. <https://doi.org/10.1016/j.atmosres.2014.07.008>
- Xu, H., Guo, J., Ceamanos, X., Roujean, J.-L., Min, M., & Carrer, D. (2016). On the influence of the diurnal variations of aerosol content to estimate direct aerosol radiative forcing using MODIS data. *Atmospheric Environment*, *141*, 186–196. <https://doi.org/10.1016/j.atmosenv.2016.06.067>
- Yoshida, M., Kikuchi, M., Nagao, T. M., Murakami, H., Nomaki, T., & Higurashi, A. (2018). Common retrieval of aerosol properties for imaging satellite sensors. *Journal of the Meteorological Society of Japan*, *96B*, 193–209. <https://doi.org/10.2151/jmsj.2018-039>
- Yu, H., Chin, M., Yuan, T., Bian, H., Remer, L. A., Prospero, J. M., et al. (2015). The fertilizing role of African dust in the Amazon rainforest: A first multiyear assessment based on data from Cloud-Aerosol Lidar and Infrared Pathfinder Satellite Observations. *Geophysical Research Letters*, *42*, 1984–1991. <https://doi.org/10.1002/2015GL063040>
- Zawadzka-Manko, O., Stachlewska, I. S., & Markowicz, K. M. (2020). Near-real-time application of SEVIRI aerosol optical depth algorithm. *Remote Sensing*, *12*, 1481. <https://doi.org/10.3390/rs12091481>
- Zhang, H., Kondragunta, S., Laszlo, I., & Zhou, M. (2020). Improving GOES Advanced Baseline Imager (ABI) aerosol optical depth (AOD) retrievals using an empirical bias correction algorithm. *Atmospheric Measurement Techniques*, *13*, 5955–5975. <https://doi.org/10.5194/amt-13-5955-2020>